An Investigation of the Effects of Hydrogen on Local Strain Fields and Structural Disorder-to-Order Transition in Hydrogenated Amorphous Silicon

Aniekan Magnus UKPONG
Department of Physics, University of Cape Town, Rondebosch 7701,
Cape Town-SOUTH AFRICA
e-mail: ukponga@science.uct.ac.za

Abstract

This study utilizes the fluctuations in the mean silicon-silicon near neighbour distances and local atomic-level stresses to study the chemically-induced disorder-to-order transition in hydrogenated amorphous silicon as a function of hydrogen concentration C_H. The correlation between a suitable stress and structure parameter shows a three-stage structure transition that culminates in the formation of a crystalline phase at high C_H. In the low C_H limit, the structural changes are characterized by a linear response to stress giving a rigidity modulus of 73.43±15 GPa. In the intermediate and high C_H limits, the stress-structure correlation shows a volume-dependence. At very high hydrogen concentrations, a high rigidity modulus is obtained in good agreement with the rigidity of crystalline silicon. An interpretation of the results in terms of the constraint counting model of the continuous random network suggests that the observed high modulus of rigidity characterizing the crystalline phase is a direct consequence of the reduction in volume fraction due to increased hydrogen bonding.

Key Words: Amorphous silicon, atomic-level stress, defects, topological disorder, local order, strain-fields.

1. Introduction

Amorphous silicon (a-Si) and hydrogenated amorphous silicon (a-Si:H) are important prototypes of tetrahedral covalent semiconductors and have drawn considerable attention because of their potentials for multiple technological applications [1, 2]. From a theoretical viewpoint, these materials are unique for testing theoretical models and validating computer experiments because of the large number of experimental studies that have been carried out over the past few decades. However, in spite of advances in their study, the inherent absence of long-range order [3], the preservation of short range order in the disordered topology, and the presence of structural defects depending on the method and conditions of film preparation have made their local structure an interesting subject of research.

In a-Si:H, topological disorder plays a significant role in determining the electronic properties [4, 5]. An obvious issue is the effect of hydrogen on the degree of disorder. The understanding of this effect is important in optimizing thin film properties for technological applications. An experimental study using Rahman scattering spectroscopy [6] showed that hydrogen causes a relaxation of the atomic network in

a-Si:H. The relaxation effect was shown to be more profound on medium range order than on short range order, and notably, relaxations in the bulk and surface regions of a-Si:H was shown to behave differently due to their different hydrogen contents. In Reference [7], a combination of molecular dynamics simulations and attenuated total-reflection Fourier transform infrared spectroscopy (ATR-FTIR) was used to study the mechanism of hydrogen-induced crystallization of a-Si:H during post deposition treatment with an $H_2(D_2)$ plasma. The study shows that crystallization is mediated by the insertion of hydrogen into strained Si-Si bonds as it diffuses through the film.

An investigation of structural ordering and intrinsic strain in a-Si:H thin films grown by hot wire chemical vapour deposition (HWCVD) method at different substrate temperatures using X-ray diffraction [8] and synchrotron radiation diffraction [9] show that intrinsic strain is mainly carried by distortions in bond angles. Further studies of the mesoscale structure [10] of a-Si:H samples prepared at different deposition temperatures reveal structural anisotropies which suggest that the distortions in bond angles may have arisen from the presence of dangling bond defects, most of which are hydrogen-terminated. Microstructural characteristics and total hydrogen content derived from FTIR spectroscopy are shown to depend on deposition temperature [11]. Nevertheless, neither the exact form of the transition from disorder to order, nor the nature of the correlations between the local strain fields and the structural order has been well-understood. Although the present study can be considered as a complement of all these earlier studies, it investigates the different stages involved in the chemically induced disorder-to-order transition in hydrogenated amorphous silicon.

In order to determine the form of the disorder-to-order transition in a-Si:H, the correlations between stress and order is investigated subject to changing concentrations of hydrogen. It is assumed that (i) an order parameter can be defined for a given structure of a-Si; and (ii) the atomic-level stresses can be characterized for a given structure. The dependence of (i) and (ii) on hydrogen concentration is utilized to study the structure transition and evolution of order. The stress-order correlations are utilized to study the elastic properties of the evolving structure. The structure of this paper is as follows. The computational methodology is presented in section 2. The procedures for preparing the pure structures, incorporation of hydrogen, and thermal equilibration of hydrogenated structures are also presented. The formalism for computing atomic level stresses using the results of the structure simulations is also presented. The main results of structure simulations and atomic stress computations are presented in section 3. The correlations between structure and stress are discussed in section 4, and conclusions are drawn in section 5.

2.   Computational Details

2.1.   Interatomic potential

The theoretical basis of the tight binding (TB) approach of simulating covalent materials has been adequately presented in References [12–15]. In this formalism, the total energy is

$$E^{total} = \sum_n \varepsilon_n - E_{rep}. \tag{1}$$

The first term describes the band structure energy. This is the quantum mechanical bonding energy arising from the overlap of atomic orbitals. The band structure energy is evaluated as a sum of the approximate energy of all occupied electronic eigenstates. The second term is a two-body potential which accounts for all other contributions to the total energy. This essentially represents the repulsive ion-ion interactions.

The parameterizations of Harrison [16] were used with the modifications provided in the Goodwin-Skinner-Pettifor (GSP) model [17] to determine the TB Hamiltonian matrix elements for Si-Si interaction. These matrix elements are determined in terms of hopping parameters as

$$H_\alpha\left(\frac{r}{r_0}\right) = H_\alpha^{Si-Si}(1)\left(\frac{r_0}{r}\right)^n exp\left\{n\left[-\left(\frac{r}{r_c}\right)^{n_v} + \left(\frac{r_0}{r_c}\right)^{n_c}\right]\right\}. \tag{2}$$

In this case, $H_\alpha^{Si-Si}(1)$ are the hopping coefficients at equilibrium Si-Si bond length r_0, and n is the hopping exponent. The repulsive interaction term has a similar form

$$\phi^{Si-Si}\left(\frac{r}{r_0}\right) = \phi^{Si-Si}(1)\left(\frac{r_0}{r}\right)^m exp\left\{m\left[-\left(\frac{r}{r_c}\right)^{m_c} + \left(\frac{r_0}{r_c}\right)^{m_c}\right]\right\}. \qquad (3)$$

The pair potential exponent m, and other parameters retain the earlier GSP form. This form of repulsive potential is known to correctly reproduce the binding energy curves of various phases of silicon obtained from first principles calculations. An important characteristic of the GSP model is that the total repulsive potential between interacting species is a nonlinear function of the sum of the repulsive pair potentials between the reference atom and its neighbours:

$$E_{rep} = \sum_i F\left(\sum_{i,j\neq i} \phi(r_j - r_i)\right), \qquad (4)$$

where $\phi(r_j - r_i)$ is the repulsive pair potential between atoms i and j, and retains the GSP scaling form. F is a polynomial used in fitting the hopping coefficient to ensure that the interatomic interactions are short-ranged and therefore preserve the bond lengths.

In a-Si:H, there are three types of ionic interactions. These are Si-Si, Si-H and H-H interactions. Li and Biswas (LB) [18] have showed that the total repulsive potential is no longer a nonlinear function of the sum of pair potentials when Si-H interactions are included. In fact it is no longer clear how much of the Si-H and H-H potentials are to be included in the operand of equation (4), and depends largely on the partitioning of the pair potentials between individual atomic species. In Reference [18] the Si-H potential has been partitioned into two parts: (i) a fraction c of the Si-H interatomic potential is added directly to the Si-Si repulsive potential, and (ii) the remaining fraction (1-c) is classified as belonging to H atoms so that the total repulsive potential is

$$E_{rep} = \sum_i F\left[\left(\sum_{i,j\neq i} \phi^{Si-Si}(r_j - r_i)\right) + c\sum_{i,k\neq i} \phi^{Si-H}(r_k - r_i)\right] + (1-c)\sum_k^H \sum_i^{Si} \phi^{Si-H}(r_k - r_i). \qquad (5)$$

The first term in equation (5) is the modified Si-Si repulsive interaction. In this case, i and j represent near neighbour silicon atoms and k denotes hydrogen atoms. The GSP model defines only the difference between the Si self-energies E_s and E_p, and not their absolute values. This important feature allows us to systematically partition the contributions to the total repulsive potential since it is no longer a linear function of the Si-Si interaction.

In order to introduce hydrogen TB parameters, some energy reference has to be chosen to preserve some well-known properties of the Si-H system. In this work, this energy reference is chosen such that: (1) If c = 0, the difference in Si self energy ΔE_{sp} is 8.295 eV and, (2) If $c > 0$, the equilibrium Si-H bond length is 1.475 Å with a Si-H binding energy of 3.33 eV, in agreement with the experimental binding energy (3.35 eV) reported in Reference [19]. The H atom has one s orbital, so that the three TB parameters consisting of the orbital energy E_s, and the magnitude of the two overlap integrals at the Si-H bond length are determined by adjusting the parameter c of the LB functional to preserve the energies of the two occupied molecular orbitals a_1^+ = -18.20 eV and t_2^+ = -12.70 eV, and the symmetric bond bending vibrational frequency of 976 cm^{-1} of the silane molecule. The resulting TB parameters for Si-H interaction are consistent with those of Kim et al. [19], with the exception of $\phi^{Si-Si}(1)$, which is obtained as 3.4581 eV, in agreement with the TB parameters of Si-Si interaction of the GSP model. A summary of the TB parameters used in this study is presented in Table 1. The choice of the LB functional for the total interatomic potential conveniently allows for a scaling of the total energy to satisfy bonding requirement in a-Si:H through the adjustable parameter c. For instance, the choice c = 0 is equivalent to the GSP model where there is only Si-Si interaction.

Table 1. Summary of TB parameters used in molecular dynamics simulations.

TB parameters	Units	Si − Si	Si-H
$H_{ss\sigma}$ (1)	eV	-1.82	-3.535
$H_{sp\sigma}$ (1)	eV	1.96	5.088
$H_{pp\sigma}$ (1)	eV	3.06	
$H_{pp\pi}$ (1)	eV	-0.87	
r_0	Å	2.35	1.48
r_c		3.67	2.19
n		2	1.972
n_c		6.48	13.27
m		4.54	2.255
m_c		6.48	13.27
ϕ(1)	eV	3.5481	3.01
E_s (Silicon)	eV	-13.08	
E_p (Silicon)	eV	-4.785	
E_s (Hydrogen)		-8.335	
c		0.0	0.12

The total number of valence electrons is set to $4 \times N_{Si} + 1 \times N_H$ and the occupied eigenstates and the corresponding eigenvectors are obtained by direct diagonalization of the tight binding (TB) Hamiltonian matrix, with appropriate corrections for double counting, in line with Pauli principles. The total energy is evaluated during the MD cycle as the sum of the band structure energy and the total repulsive energy. The total energy and forces are evaluated at every MD step of the simulation to search for suitable global energy minimum before properties of the system were computed.

2.2. Structure simulations

The simulation starts with an initial cell of 1728 silicon atoms placed in a perfectly ordered diamond lattice at 300 K. The size of the MD cell is set to 10å × 10å × 10å, where å = 5.429 Å is the lattice parameter of silicon. This choice sets the density to 2.33 gcm^{-3}, which corresponds to the experimental value of c-Si [20]. The initial cell is heated to 3000 K in a constant temperature (NVT) simulation in the canonical ensemble scheme, where the velocity and kinetic energy of ionic motion are constantly rescaled to the simulation temperature. The resulting Newton's equations of motion are integrated using the velocity form of the Verlet algorithm [21] with a time step Δt =1 fs. The hot melt is equilibrated for 2 ps over 2000 MD time steps over which a structure with the minimum total energy is obtained. The resulting structure is then quenched from 3000 K to 300 K at the rate of 2.7×10^{17} K/sec over 10 ps. It is then annealed to a temperature of 1500 K over a time of 1ps to ensure that the resulting a-Si structure loses memory of its crystallinity before cooling down to 300 K. The total energy of the resulting a-Si is minimized over 50000 MD time steps and the structure is equilibrated at 300 K, until a stable structure is obtained. For this structure, changes in total energy are less than 6.21×10^{-2} meV.

Using the resulting atomic coordinates of the equilibrated pure structure, hydrogen is selectively incorporated into the network using the technique of Reference [22]. The number of hydrogen N_H is set to 52, 86, 138, 173, 225, 259, 311, 346, 397 and 432 in each case, and the corresponding number of silicon atoms N_{Si} is correspondingly reduced to 1676, 1642, 1590, 1555, 1503, 1469, 1417, 1382, 1331 and 1296. These correspond to a-Si:H with percentage atomic hydrogen concentration of 3%, 5%, 8%, 10%, 13%, 15%, 18%, 20%, 23% and 25% respectively. As a result of the small activation energy of hydrogen migration in pure a-Si relative to the strength of the Si-H bond [23, 24], the hydrogenated structure is neither heated nor cooled, rather, a suitable algorithm is used to relax the hydrogenated structure at 300 K. Finite energy (NVE)

MD simulation is performed within the microcanonical ensemble scheme to minimize the total energy at constant volume and particle number of the hydrogenated structures over 150000 time steps in search for global energy minimum. These structures are stable at 300 K, with variations in total energy less than 0.04 meV compared to the thermal energy of 38.76 meV. These levels of hydrogen are consistent with typical a-Si:H films [25, 26].

2.3.   Atomic-level stresses

The content of this section is closely followed by Kelires's paper [27]. In a macroscopically rigid body under no external forces, the local stress is considered to arise from local incompatibilities, which are present in disordered networks of amorphous silicon and in any network with non-equivalent atoms. For instance, if an atom does not fit ideally into the environment where it is placed, atomic-level stresses will result. Following arguments analogous to those used in the derivation of the Hellmann-Feynman force theorem [28], Nielsen and Martin [29, 30] showed that the total macroscopic stress can be expressed as a sum of the expectation values of certain operators defined at individual atoms, so that if the Hamiltonian (without including external perturbations) is given by

$$H = \sum_i \frac{P_i^2}{2m_i} + V_{int}. \tag{6}$$

where P_i is the momentum operator, m_i is the mass of the i-th atom and V_{int} is the interaction between the atoms in the system. The total stress is then given by

$$\sigma^{\alpha\beta} = \sum_i \left\langle \psi \left| r_i^\beta \frac{dV_{int}}{dr_i^\alpha} - \frac{P_i^\alpha P_i^\beta}{m_i} \right| \psi \right\rangle, \tag{7}$$

where α and β are the Cartesian coordinates. In this case, $r_i^{\alpha(\beta)}$ and $P_i^{\alpha(\beta)}$ are the $\alpha(\beta)$ components of the position and momentum of the $i-$th atom, respectively, and ψ is the exact eigenfunction of the Hamiltonian. Nielsen and Martin defined a local strain field in a system of atoms $\sigma^{\alpha\beta}(\vec{r})$, such that $\int \sigma^{\alpha\beta}(\vec{r}) d(\vec{r})$ over the supercell volume is equal to the total stress given by equation (7). This stress field is defined at each point in space on the nuclei and the electrons, and is considered as the expectation value of the linear term in the expansion of the Hamiltonian with respect to an infinitesimal virtual strain $\varepsilon^{\alpha\beta}$.

However, in order to study the local atomic structure of amorphous silicon, it is more convenient to define the stress averaged over an appropriate atomic volume. Following Reference [27], the atomic-level stress tensor associated with any atom i, located at position $\boldsymbol{r}_i$ inside the simulation box is defined as

$$\sigma^{\alpha\beta}(i) = \frac{1}{\Omega_i} \int \sigma^{\alpha\beta}(\vec{r}) d\vec{r}, \tag{8}$$

where the integral extends over the atomic volume. The total stress given in equation (7) is then

$$\sigma^{\alpha\beta} = \sum_i \Omega_i \sigma^{\alpha\beta}(i). \tag{9}$$

In practice, the evaluation of atomic-level stress tensors depends on the method of calculating the total energy of the system. In this study, the tight binding approach is used to compute total energy and forces, however, methods based on either the density functional theory, embedded atom method or pair potentials can also be used. The atomic coordinates, forces and velocities obtained from the TBMD simulations are used as input parameters in the atomic-level stress tensor computation. The block diagram of the computational procedures is presented in Figure 1. These tensors are computed using the approach outlined by Egami et al. [31]. We assume that the interatomic potential is a smooth function of inter-atomic separation r_{ij}, and

write the stress-tensor as

$$\sigma^{\alpha\beta}(i) = -\frac{1}{\Omega_i}\left[\frac{1}{2}\sum_j F_{ij}^\alpha r_{ij}^\beta + m_i v_i^\alpha v_i^\beta\right],\tag{10}$$

where $\boldsymbol{F}_{ij}$ is the force on atom i due to atom j, m_i is the mass of atom i and $\boldsymbol{v}_i$ is the velocity of atom i. Therefore for any atom i in the simulation box, $\sigma^{\alpha\beta}(i)$ becomes a non-local property of the state of the material in the neighbourhood of that atom because the interatomic potential has a finite range. The atomic-level stresses are treated as local responses of the atomic system to infinitesimal virtual strains $\varepsilon^{\alpha\beta}$ due to the forces F_{ij}^α at atomic sites. A map of $\sigma^{\alpha\beta}(i)$ in space can provide information on the size of a defect site, local structure modifications due to these defect and site symmetries in a given disordered topology of a-Si:H.
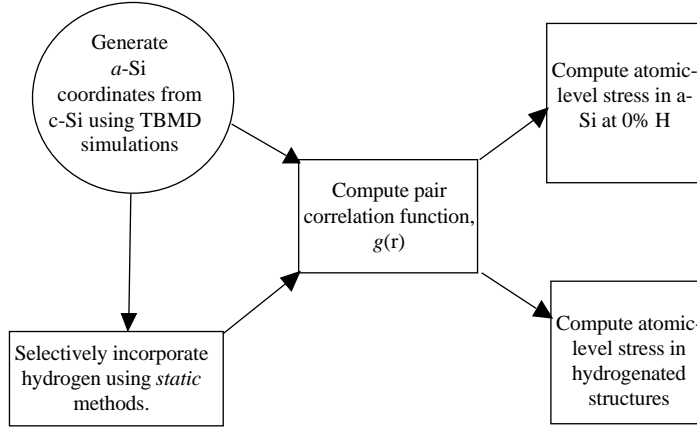
Figure 1. Block diagram of computer implementation procedures.

3.   Results

The evolution of the equilibrated structures is presented in terms of the Si-Si pair correlation function in Figure 2 as a function of hydrogen concentration, C_H. From Figure 2, the minimum first near-neighbour correlation distance is 2.14Å at all levels of hydrogen. Within a 5.0 Å correlation distance, only the first and second neighbour coordination peaks are observed at low C_H. The low C_H limit is characterized by a complete disappearance of the third coordination peak. There is a splitting of the second coordination peak to form a shoulder on the second peak at 4.50 Å when C_H is increased from 8% to 10%. This shoulder gradually evolves into the third peak as C_H is increased from 10% to 18%. This evolution is complete at 20% H when the third peak is centred at 4.45 Å. Further increase in C_H from 20% to 25% does not change the peak characteristics. In the low C_H limit, there is only one broad peak centred at about 6.75 Å beyond a correlation distance of 5.0 Å. At intermediate concentrations (10–18%), the broad peak evolves into four distinct peaks with centres at 5.0 Å, 5.9 Å, 6.8 Å and 7.6Å respectively. As C_H increases further from 18% to 20%, the number of coordination peaks appearing in this long range limits increases to six. Two additional peaks appear as a result of the splitting of each of 5.9 Å and 6.8 Å peaks. Neither the number of coordination peaks appearing in this long-range correlation distance nor their mean positions are changed when C_H is further increased from 20%–25%, however, the height and intensity of the peaks are constantly increased as C_H increases.
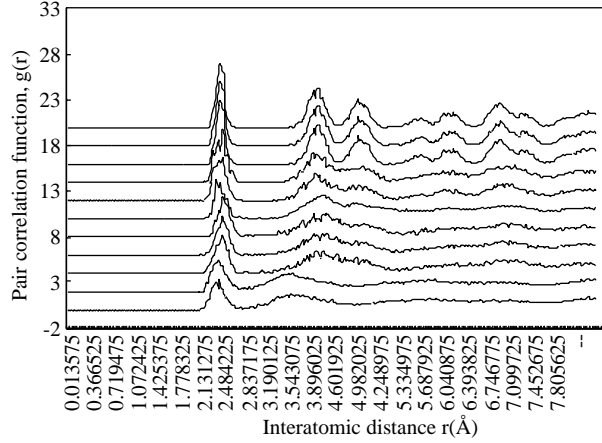
Figure 2. Si-Si pair correlation function, $g(r)$ showing the structure evolution with hydrogen concentration C_H.

The pair correlation function of c-Si exhibits peaks that correspond to a sequence of coordination shells that is characteristic of the presence of short and long range order. A detailed structural analysis of the pair correlation function for different structures clearly shows a transformation of the amorphous structure to a crystalline structure at higher C_H. A suitable parameter is required to estimate the degree of order with changing C_H. Assuming that the coordination peaks can be represented by a normal probability distribution, the full width at half maximum (FWHM) of the distribution could serve as a good measure of the evolving order because it measures of the deviations from the mean peak position of the distribution. A Gaussian fit to the coordination peaks, show that mean peak positions decrease from 2.42 Å to 2.35 Å as the structure relaxes. Figure 3 shows the variations in the FWHM of the first coordination peak with C_H. The FWHM drops rapidly as C_H increases from 0–15%. The decrease is slow as C_H increases from 15–20%, and remains unchanged up to 25%.
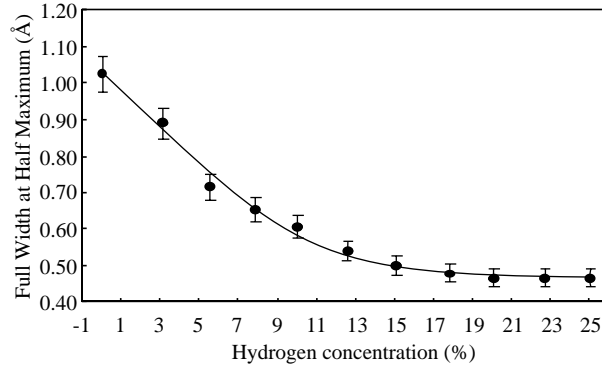
Figure 3. The correlation of the FWHM of first coordination peak with percentage hydrogen concentration C_H.

It is quite important to study how many atoms surround a given Si atom in the simulated structures as the structure relaxes towards crystallization. This is given by the coordination number, z. From $g(r)$, a preliminary coordination number can be obtained by integrating over a specified interval (r-δr, r+δr) around pronounced peaks

$$z = \int\limits_{r-\delta r}^{r+\delta r} 4\pi r^2 \rho(r) dr. \tag{11}$$

The integration of the maximum yields the coordination number. The area under the near-neighbour coordination peak is approximately equal to $4\pi r^2 \rho(r)$, where $\rho(r)$ is the atomic density within a spherical volume

of radius r, and dr is the width of the Gaussian peak. The variations in the mean number of first and second nearest neighbours with changing levels of hydrogen are presented in Figure 4. The average numbers of first and second nearest neighbours decreases slowly toward their value in c-Si as hydrogen concentration increases steadily to 25%.
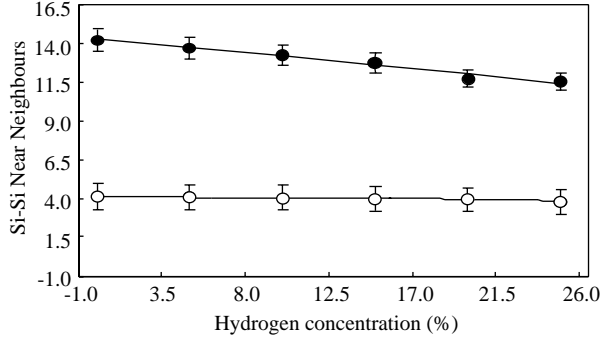
Figure 4. First nearest neighbours (open symbols) z_1, and second nearest neighbours (solid symbol) z_2 as a function of hydrogen content.

The random distribution of atomic sites in a-Si:H necessitates a statistical treatment of the atomic-level stresses. The snapshot of atomic-level stress in the simulated structures is presented in Figure 5. The histograms show a decreasing mean stress as C_H increases. The root mean square (RMS) stress is used as a measure of the spread in the stress at different sites. Figure 6 shows the dependence of RMS stress on C_H. Similar to the dependence of the FWHM on C_H, the dependence of the RMS stress on C_H, shown in Figure 6 is clearly non-linear. In contrast with the FWHM, at high hydrogen concentrations, there are small changes in the spread of the stress even though there are no appreciable structural changes. In Table 2, the total stress and the RMS stress are also shown to decrease with increasing hydrogen content.

Table 2. Statistical analysis of stress parameters showing a decrease in bulk stress with increasing hydrogen content.

C_H (%)	Stress range (KPa)	Mean stress (KPa)	Total stress (MPa)	Mean square stress (KPa)^2	RMS stress (KPa)
0	16.30	0.502	0.860	9.031	3.005
3	13.3	0.149	0.707	5.377	2.319
5	12.00	0.149	0.258	2.559	1.612
8	11.2	0.137	0.236	1.728	1.315
10	10.50	0.103	0.178	1.278	1.130
13	7.5	0.002	2.61×10^{-2}	0.337	0.581
15	2.52	2.71×10^{-4}	4.63×10^{-4}	0.1261	0.356
18	1.82	4.63×10^{-4}	8.00×10^{-4}	0.077	0.277
20	0.55	4.63×10^{-4}	8.00×10^{-4}	0.0057	0.076
23	0.52	4.63×10^{-4}	8.00×10^{-4}	0.0054	0.073
25	0.52	4.63×10^{-4}	8.00×10^{-4}	0.0052	0.0721

Figure 7 shows the correlations between local contributions to stress and structural order. The plot of RMS stress as a function of the FWHM on a log-log scale clearly reveals a three-stage disorder-to-order transition. At the low C_H limit (stage 1), a one-to-one correlation exists between stress and structural order. This suggests a linear elastic response of the structure to stress in line with Hooke's law. From Figure 7, the

Young's modulus for the three transition stages give $Y(1) = 73.43 \pm 15$ GPa, $Y(2) = 36.72 \pm 2.86$ GPa and $Y(3) = 158 \pm 20$ GPa. Within error bounds, the calculated value of $Y(1)$ agrees very well with the value of 80 ± 20 GPa [32]. At the high C_H limit (stage 3), the large slope is indicates that the structure sensitivity to stress is non-linear. The decrease in stress from stage 1 to stage 2 with increasing hydrogen is clear evidence of some local structure rearrangements. These rearrangements are characterized by a decrease in stress and the onset of local structure ordering. In stage 2, where C_H increases from 10% to 20%, the stress-structure correlation obeys a power law, varying linearly with the cubic power of the FWHM. The slope of 3.0 for stage 2 is clear evidence of a volume dependence of the stress.
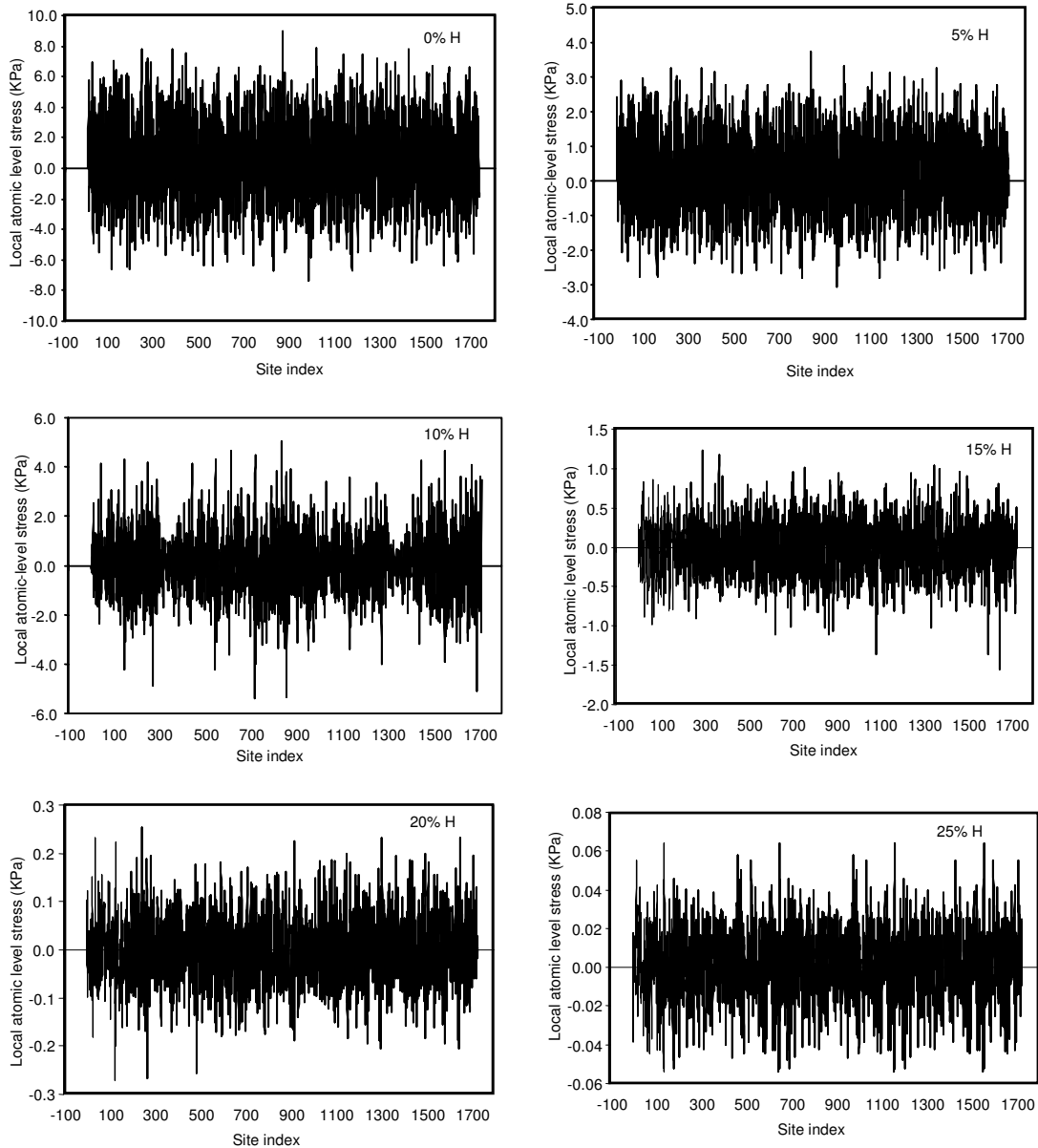
Figure 5. Snapshots of the atomic-level stresses in hydrogenated amorphous silicon network averaged over configurations with (a) 0% H (b) 5% H (c) 10% H (d) 15% H (e) 20% H and (f) 25% H to show stress relaxation by progressive incorporation of hydrogen.
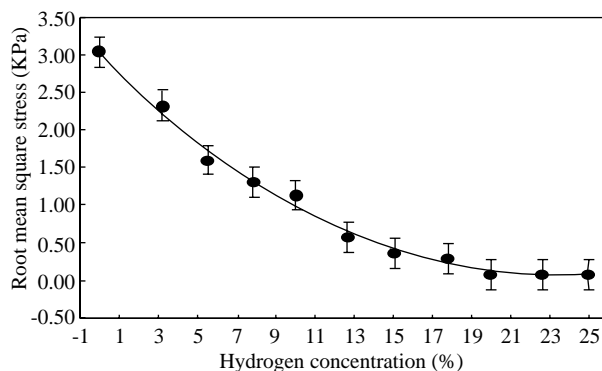
Figure 6. Dependence of root mean square (RMS) stress in hydrogenated amorphous silicon with hydrogen concentration C_H.
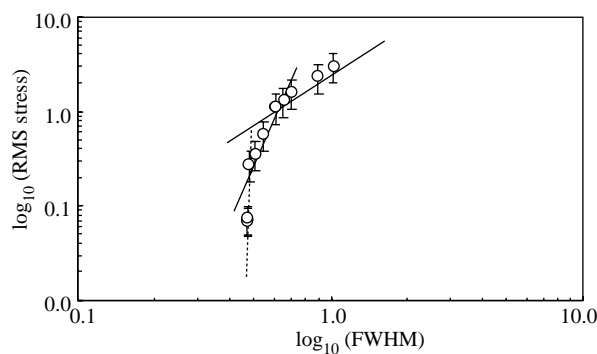
Figure 7. Evolution of the correlation between the root mean square stress ($\log_{10}\sigma$) with the full width at half maximum ($\log_{10}$(FWHM)) showing a three-stage structure transition.

4.   Discussion

Although the reliability of the quantum-mechanical description of bonding in a-Si:H is undisputed, it is still useful to provide an approximate scheme for identifying and characterizing the bonding environment in a-Si:H. To this end, a TBMD simulation has been performed to study the formation of typical a-Si:H networks, and to study the local contributions to stress and the network rearrangements induced by progressive incorporation of hydrogen. At a cutoff distance of 2.80 Å, the repulsive term in the interatomic potential dominates the Si-Si interaction, giving rise to unphysical results. The pair correlation functions discussed here was computed using a cutoff of 3.50 Å.

The pair correlation function $g(r)$ is a good measure of the probability of finding atoms within a given radial distance r from a reference silicon atom. From the shapes of $g(r)$, a perfectly ordered structure is characterized by well-defined, sharp, narrow and well-separated peaks with all coordination peaks having a zero background. Conversely, a disordered structure is characterized by broad peaks, with unequal and non-zero background. The pair correlation function averaged over 11 configurations is confined to a radial distance of 8.0 Å. From the profiles of Figure 2, the networks become more ordered as hydrogen is incorporated progressively. The analysis of the simulated structures in terms of Gaussian fits to pronounced coordination peaks using Microcal Origin v5.0 gives the integral area, peak centre, Gaussian width, offset or background correction, Gaussian peak height, and full width at half maximum (FWHM).

When compared with the c-Si pair correlation function averaged over an 8 Å radius, the number of evolving coordination peaks increases steadily from three to nine as C_H increases from 0–25%. In terms of the Gauss fit parameters, the centre of a given peak corresponds to the mean nearest neighbour distance and the area of the peak is an approximate measure of the number of nearest neighbours available within a given radial distance from a reference atom. The Gaussian width gives a measure of the fluctuations in the mean nearest neighbour distances. The FWHM of a given coordination peak is a measure of the average fluctuation in the mean nearest neighbour distance at half maximum pair correlation. The FWHM is a good measure of order since well-separated and narrow peaks have very small Gaussian widths. A small FWHM reflects small deviations in the mean positions of nearest neighbours and shows that the structure is ordered, and vice versa. Although the mean peak positions are observed to decrease with increasing hydrogen concentration, the use of the FWHM as a measure of order eliminates the errors associated with utilizing the absolute values of the peak positions as an order parameter.

The formation of second and third nearest neighbours with increasing C_H is also an indication of structural changes that result in ordering. A measure of the probability of formation of nearest neighbours is obtained from the intensities of a given coordination peak in g(r). The effect of hydrogen on the structure is clearly seen in terms of the increases in the Gaussian intensity of a given peak after progressive hydrogenation relative to the hydrogen-free structure. Table 3 shows the Gaussian fitting parameters of the pronounced peaks in g(r) with changing C_H. It is found that as C_H is increased, the average position of the centre of the first two coordination peaks decreases towards the equivalent values in c-Si. From Table 3, the Gaussian intensities of the first and second peaks increase steadily, however, the width of these peaks decreases steadily with increasing C_H.

Table 3. Gauss fit parameters of the first and second pronounced peaks in $g(r)$: Effects of hydrogen content C_H.

Hydrogen content (%)	First coordination peak			Second coordination peak		
	Area ($Å^2$)	Center (Å)	Width (Å)	Area ($Å^2$)	Center (Å)	Width (Å)
0	1.039	2.4623	0.5917	1.5044	4.2234	0.8703
3	1.165	2.4221	0.4718	1.7261	4.1420	0.8471
5	1.212	2.3816	0.4507	1.9299	4.0741	0.81611
8	1.512	2.3766	0.4271	1.9533	4.0328	0.77426
10	1.564	2.3691	0.4177	1.9863	4.0207	0.7556
13	1.577	2.3649	0.3136	2.2101	3.9238	0.73136
15	2.108	2.3617	0.2596	2.1952	3.8583	0.67695
18	2.685	2.3585	0.2057	2.3064	3.8497	0.62057
20	2.751	2.3546	0.1978	2.7274	3.8349	0.45652
23	2.751	2.3546	0.1978	2.7274	3.8349	0.45652
25	2.751	2.3546	0.1978	2.7274	3.8349	0.45652

The parameters that characterize short range order are extracted from the computed pair correlation functions g(r). These are the average fluctuations in the mean first-, second-, and third nearest neighbour distances r_1, r_2 and r_3, the first and second neighbour coordination number z_1 and z_2, and the average triplet correlation angle θ, (θ is the angle between a central silicon atom and its two nearest neighbours). In terms of these parameters, perfect short range order is characterized by a mean first and second neighbour distances of 2.35 Å and 3.85 Å with corresponding coordination numbers of 4.0 and 12.0, and a triplet atom correlation angle, θ corresponding to the tetrahedral angle of 108.28°. Figure 4 shows the deviation of z_1 and z_2 from the c-Si values as a function of C_H. These deviations towards the limiting values in c-Si give an estimate of order in the evolving structures. The preservation of local short range order and evolution of

first and second near neighbour bonding geometries provide ancillary evidence that a decreasing RMS stress leads to a corresponding increase in structural order.

Taken together, the observed changes in FWHM in Figure 3 and average first and second neighbour distances in Figure 4 cannot occur without affecting the local structure, at least at correlation distances longer than 4.5 Å. The evolution of long-range order is characterized by the appearance of third, fourth and higher coordination peaks, which is attributable to hydrogen induced crystallization of a-Si:H. The number of first Si-Si near neighbours computed using Equation. (11), and its dependence on hydrogen concentration (Figure 4) agrees excellently with the estimates in Reference [33] for a Si-H system. A similar behaviour is obtained for Ge-H systems studied experimentally using extended X-ray absorption fine structure [34]. In this study, we assume that the average first nearest neighbour coordination Z_1 is modelled as,

$$Z_1 = 4 - \frac{C_H}{100 - C_H}, \tag{12}$$

where C_H is in percent (%). This estimate assumes that the number of dangling bonds is negligible in the network compared with the number of Si-H bonds. This is true due to the role of hydrogen in passivating dangling bonds. If the Si-H bonds do not contribute to structural rigidity in a-Si:H, the Young's modulus should decrease as Z_1 decreases, because a decreasing Z_1 implies that less number of Si atoms are interconnected. Assuming that the local network structure of a-Si:H can be modelled in terms of the continuous random network (CRN) of silicon atoms [35], with hydrogen acting as a substitutional impurity, then the Young's modulus of a-Si:H can be evaluated in terms of the constraint-counting model (CCM) of the CRN [36–38]. In Refs. [39, 40], elastic properties of covalent glasses has been evaluated as a function of the first nearest neighbour coordination number Z_1 as,

$$Y = Y_{c-Si} \left(\frac{Z_1 - r_0}{4 - r_0} \right)^{1.5}, \tag{13}$$

where Y_{c-Si} is the Young's modulus of crystalline silicon and $r_0 = 2.4$ is the percolation threshold, beyond which the network becomes floppy. From equation (12), a decreasing Z_1 corresponds with an increasing C_H, for which the CCM predicts a uniform decrease in Young's modulus as C_H increases.

The usefulness of atomic-level stresses in characterizing the local structure of amorphous solids has been summarized by Vitek and Egami [41]. From Figure 5, a decreasing mean stress and mean square stress with increasing C_H is in direct agreement with the experimental observations in Reference [42], where a uniform decrease in the intrinsic compressive stress in samples of a-Si:H is observed to correspond with increasing hydrogen concentration. In Figure 6, the exponential dependence of the mean square stress on C_H alludes to a decreasing mean stress with increasing C_H. A similar dependence in FWHM suggests that there may be a one-to-one correspondence between structure and stress. This is confirmed in regions (1) and (2) of Figure 7, where the observed decrease in Y agrees well with the CCM. The disagreement of the Young modulus with the CCM in region (3) is clear evidence that the stress states is non-uniform in a-Si:H. The high value of $Y(3)$ is indicative of the crystallinity observed in that region. This is consistent with the role hydrogen plays in increasing the packing fraction as more hydrogen is incorporated into the CRN.

5.   Conclusion

A tight binding molecular dynamics simulation has been performed to study the local strain fields and evolution of structural order in hydrogenated amorphous silicon. The results show that increasing the hydrogen content causes a corresponding decrease in the mean square stress, and leads to the relaxation of the amorphous silicon network towards crystallization in general agreement with experimental observations. The correlation between the order parameter and the stress parameter shows a three-stage disorder-to-order structure transition, with hydrogen playing a dominant role. The linear response of the structure to stress

implies that Hooke's law is satisfied in a-Si:H at low C_H limit. This suggests that the atomic-forces giving rise to the atomic-stresses arise from harmonic potentials. At intermediate hydrogen concentrations, the volume dependence of the stress is clear evidence of the increase in packing fraction, and perhaps a change in macroscopic density. At the upper limit of C_H, the insensitivity of the structure to stress gives rise to very high rigidity modulus, which suggests that extra hydrogen goes into relieving the bond strain and contributes to network rigidity contrary to the assumptions of the constraint counting model.

Acknowledgments

References

[1] R. A. Street, *Hydrogenated amorphous silicon* (Cambridge University Press, Cambridge, 1991) p. 25.

[2] K. Tanaka, E. Maruyama, T. Shimada, H. Okamoto, *Amorphous silicon* (John Wiley and Sons, West Sussex, England, 1999) p. 219.

[3] N. E. Cusack, *Physics of structurally disordered matter* (IOP Publishing Ltd., Bristol, 1987) p.12.

[4] P. Ordejón, E. Martnez, and F. Ynduráin, *Phys. Rev.,* **B40**, (1989), 12416.

[5] A. Aljishi, J. D. Cohen, S. Jin, and L. Ley, *Phys. Rev. Lett.*, **64**, (1990), 2811.

[6] S. Gupta, R. S. Katiyar, G. Morrell, S. Z. Weisz and I. Balberg, *Appl. Phys. Lett.*, **75**, (1999), 2803.

[7] S. Sriraman, S. Agarwal, E. S. Aydil and D. Maroudas, *Nature*, **418**, (2002), 62.

[8] M. Härting, D. T. Britton, R. Bucher, E. Minani, A. Hempel, M. Hempel, T. P. Ntsoane, C. Arendse, and D. Knoesen, *J. Non-Cryst. Solids*, **299-302**, (2002), 103.

[9] M. Härting, D. T. Britton, E. Minani, T. P. Ntsoane, M. Topic, T. Thovhogi, O. M. Osiele, D. Knoesen, S. Harindintwari, F. Furlan and C. Giles, *Thin Solid Films*, **501**, (2006), 75.

[10] D. T. Britton, E. Minani, D. Knoesen, H. Schut, S. Eijt, F. Furlan, C. Giles and M. Härting, *App. Surf. Sci.*, **252**, (2006), 3194.

[11] P. Danesh, B. Pantchev, K. Antonova, E. Liarokapis, B. Schmidt, D. Grambole, and J. Baran, *J. Phys. D: Appl. Phys.*, **37**, (2004), 249.

[12] L. Colombo, *Annual reviews of computational physics*, ed. D. Stauffer, Vol. 4, (World Scientific, Singapore, 1996) p. 147.

[13] C. M. Goringe, D. R. Bowler and E. Hernandez, *Rep. Prog. Phys.*, **60**, (1997), 1447.

[14] L. J. Lewis and N. Mousseau, *Comput. Mater. Sci.*, **12**, (1998), 210.

[15] J. Ortega, *Comput. Mater. Sci.*, **12**, (1998), 192.

[16] W. A. Harrison, *Electronic structure and the properties of solids* (Freeman, San Francisco, 1980) p. 48.

[17] L. Goodwin, A. J. Skinner and D. G. Pettifor, *Europhys. Lett.,* **9**, (1989), 701.

[18] Q. Li and R. Biswas, *Phys. Rev.,* **B50**, (1994), 18090.

[19] E. Kim, Y. H. Lee and J. M. Lee, *J. Phys.: Condens. Matter*, **6**, (1994), 9561.

[20] G. E. McGuire, *Semiconductor materials and process technology handbook* (William Andrew Publishing, Noyes, 1988).

[21] M. P. Allen and D. J. Tidesley, *Computer simulation of liquid* (Clarendon, Oxford, 1987).

[22] J. M. Holender, G. J. Morgan and R. Jones, *Phys. Rev.,* **B47**, (1993), 3991.

[23] C. G. Van de Walle and R. A. Street, *Phys. Rev.,* **B51**, (1995), 10615.

[24] Y. S. Su and S. T. Pantelides, *Phys. Rev. Lett.*, **88**, (2002), 165503.

[25] K. A. Kilian and J. B. Adams, *Modelling Simul. Mater. Sci. Eng.*, **5**, (1997), 549.

[26] J. R. Abelson, *Appl. Phys.,* **A56**, (1993), 493.

[27] P. C. Kelires, *Int. J. Mod. Phy.,* **B14**, (2000), 256.

[28] R. P. Feynman, *Phys. Rev.*, **56**, (1939), 340.

[29] O. H. Nielsen and R. M. Martin, *Phys. Rev. Lett.*, **50**, (1983), 697.

[30] O. H. Nielsen and R. M. Martin, *Phys. Rev.,* **B32**, (1985), 3780.

[31] T. Egami, K. Maeda and V. Vitek, *Phil. Mag.,* **A41**, (1980), 883.

[32] L. B. Freund and S. Suresh, *Thin film materials* (Cambridge University Press, Cambridge, 2003) p. 96.

[33] S. Minomura, *Semiconductors and semimetals*, ed. J. I. Pankove, Vol. **21A** (Academic press, London, 1984) p.18.

[34] G. Dalba, P. Fornasini, R. Grisenti, F. Rocca, I. Chambouleyron and C. F. O. Graeff, *J. Phys.: Condens. Matter*, **9,** (1997), 5875.

[35] W. H. Zachariasen, *J. Am. Chem. Soc.*, **54**, (1932), 3841.

[36] J. C. Phillips, *J. Non-Cryst. Solids*, **34**, (1979), 153.

[37] J. C. Phillips, *J. Non-Cryst. Solids*, **43**, (1981), 37.

[38] M. F. Thorpe, *J. Non-Cryst. Solids*, **57**, (1983), 355.

[39] H. He and M. F. Thorpe, *Phys. Rev. Lett.*, **54**, (1985), 2107.

[40] J. Robertson, *Phys. Rev. Lett.*, **68**, (1992), 220.

[41] V. Vitek and T. Egami, *Phys. Stat. Sol.,* **B144**, (1987), 145.

[42] E. Spanakis, E. Stratakis, P. Tzanetakis and Q. Wang, *J. Appl. Phys.*, **89**, (2001), 4294.